



Article

Impact of Temperature Variations on Torque Capacity in Shrink-Fit Junctions of Water-Jacketed Permanent Magnet Synchronous Motors (PMSMs)

David Sebastian Puma-Benavides ^{1,*}, Luis Mixquititla-Casbis ², Edilberto Antonio Llanes-Cedeño ^{3,*}
and Juan Carlos Jima-Matailo ⁴

¹ School of Engineering and Science, Tecnológico de Monterrey, Puebla Campus, Monterrey 72453, Mexico

² Independent Researcher, Puebla 74160, Mexico; lmixcasbis@gmail.com

³ Faculty of Architecture and Engineering, Department of Mechanics, Universidad Internacional SEK, Carcelen Campus, Quito 170120, Ecuador

⁴ Higher Technology Degree in Automotive Mechanics, Instituto Superior Tecnológico Loja, Loja Campus, Loja 110150, Ecuador; jcjima@tecnologicoloja.edu.ec

* Correspondence: sebastian.puma@tec.mx (D.S.P.-B.); antonio.llanes@uisek.edu.ec (E.A.L.-C.)

Abstract: This study investigates the impact of temperature variations on the torque capacity of shrink-fit junctions in water-jacketed permanent magnet synchronous motors. Focusing on both baseline and improved designs; torque capacities were evaluated across a temperature range from $-40\text{ }^{\circ}\text{C}$ to $120\text{ }^{\circ}\text{C}$ under different material conditions: Least material condition, nominal, and maximum material condition. The baseline design exhibited torque capacities from 7648 Nm to 9032 Nm at $-40\text{ }^{\circ}\text{C}$, decreasing significantly to 549 Nm to 1533 Nm at $120\text{ }^{\circ}\text{C}$. The improved design showed enhanced performance, with torque capacities ranging from 8055 Nm to 9247 Nm at $-40\text{ }^{\circ}\text{C}$ and from 842 Nm to 1618 Nm at $120\text{ }^{\circ}\text{C}$. The maximum improvement was observed at $120\text{ }^{\circ}\text{C}$ for least material conditions, with a 55.4% increase, and the minimum improvement at $-40\text{ }^{\circ}\text{C}$ for maximum material conditions, with a 2.4% increase. Our findings demonstrate a significant increase in torque capacity by up to 20% under varied thermal conditions. These results underscore the effectiveness of design modifications in enhancing thermal stability and torque capacity, making the improved design a more reliable choice for high-performance applications subject to significant thermal fluctuations. This research highlights the critical role of material selection, thermal management, and precise design adjustments in optimizing the performance and reliability of permanent magnet synchronous motors.

Keywords: torque capacity; PMSMs; shrink-fit process; water jacket; interference; temperature incidence



Citation: Puma-Benavides, D.S.; Mixquititla-Casbis, L.; Llanes-Cedeño, E.A.; Jima-Matailo, J.C. Impact of Temperature Variations on Torque Capacity in Shrink-Fit Junctions of Water-Jacketed Permanent Magnet Synchronous Motors (PMSMs). *World Electr. Veh. J.* **2024**, *15*, 282. <https://doi.org/10.3390/wevj15070282>

Academic Editor: Peter Van den Bossche

Received: 25 May 2024

Revised: 16 June 2024

Accepted: 17 June 2024

Published: 25 June 2024



Copyright: © 2024 by the authors. Licensee MDPI, Basel, Switzerland. This article is an open access article distributed under the terms and conditions of the Creative Commons Attribution (CC BY) license (<https://creativecommons.org/licenses/by/4.0/>).

1. Introduction

Permanent magnet synchronous motors (PMSMs) have become integral components in various industrial and automotive applications [1] due to their high efficiency, high power density, and excellent torque characteristics [2]. The torque capacity of a PMSM is a critical factor that determines its suitability for demanding applications such as electric vehicles (EVs), wind turbines [3], and industrial automation systems. However, enhancing the torque capacity of PMSMs involves complex considerations, including thermal management, material properties, and mechanical design.

The torque capacity of PMSMs is significantly influenced by temperature; it affects both the magnetic properties of the permanent magnets and the electrical properties of the motor windings [4]. Elevated temperatures can lead to demagnetization of the permanent magnets and increased resistance in the windings, reducing the overall efficiency and torque output [5]. Effective thermal management strategies include the use of water jackets. For cooling, they are essential to maintaining optimal motor performance.

One notable mechanical design feature in PMSMs is the shrink-fit, and the crucial part is the interference between components and how these interferences are analyzed [6]; in this specific case, the water jacket and the stator stack. This assembly technique ensures a secure and efficient thermal connection, enhancing the motor's cooling efficiency. The shrink-fit method not only aids in better heat transfer but also contributes to the structural integrity of the motor, which is crucial for maintaining high torque output under varying operational conditions.

Permanent magnet synchronous motors (PMSMs) are preferred over other motor technologies such as induction motors (IMs) and brushed DC motors for several reasons. PMSMs offer higher efficiency and better power density due to the direct integration of magnets on the rotor, which reduces energy loss found in the excitation of IMs. Furthermore, PMSMs provide greater precision in speed and position control, which is essential for applications requiring dynamic response and fine movement control. According to Dambrauskas et al. (2020), PMSMs show an efficiency improvement of up to 5% over IMs, especially under variable speed conditions [7]. Additionally, the durability and lower maintenance of PMSMs, as reported by König (2023), makes them more suitable for long-term applications, reducing the total cost of ownership [8].

This highlights the importance of motor design optimization not only at the high level, when all the power train is considered, taking into account the use of a gear box [9–11] or a complex transmission, but also at a low level, considering all the components' designs [12,13], improving the thermal management [14–16], use of oil spray cooling [17], advanced materials, and efficient control strategies in improving torque capacity. By addressing various aspects such as electromagnetic design [18,19], stator winding configurations, material properties, improvements in cooling, and sustainable practices, these studies contribute to the development of motors with enhanced torque performance and efficiency.

Historically, research into the thermal stabilization of PMSMs has focused on enhancing cooling systems and refining material compositions. Park et al. (2023) and Venkatasubramanian and Shanthi (2019) explored advanced cooling techniques like direct slot cooling (DSC) and optimized indirect matrix converters, improving heat dissipation but not addressing long-term efficiency degradation [16,20]. Additionally, Zhou et al. (2023) utilized modified fuzzy particle swarm optimization (MDFPSO) for parameter identification to enhance thermal performance, though scalability and cost-effectiveness remain challenges [21]. Broader studies on thermal management in electronics and mechanical systems offer valuable insights. Liu et al. (2023) highlighted the importance of effective thermal management systems in electric vehicles, while McMillan et al. (2023) emphasized innovative cooling techniques and materials for enhancing device reliability and lifespan [6,22]. Research by Sharma et al. (2023) and Selema et al. (2022) explored advanced composite materials and optimized winding configurations to improve motor efficiency and thermal resilience [23,24]. However, these studies often overlook the integration of thermal management with motor design optimization, indicating a need for holistic approaches to stabilize PMSM characteristics across various operating conditions.

1.1. Goal Definition and Scope

The objective of the article and the research developed focuses on the influence of temperature and how it can affect the torque capacity; the torque capacity is measured between the water jacket and the stator laminations.

The analyzed electric motor is a permanent magnet synchronous motor, commonly used in automotive applications.

A permanent magnet synchronous motor (PMSM) comprises a stator, typically with copper windings, and a rotor containing permanent magnets, usually made of materials like neodymium iron boron or samarium cobalt. The stator generates a rotating magnetic field when an alternating current is applied, interacting with the permanent magnets in the rotor to produce motion. A shaft connects the rotor to the load, supported by bearings within the motor housing, which also encloses and protects the internal components. Additionally,

there may be a cooling system to dissipate heat, and a terminal box for electrical connections. Together, these components facilitate the conversion of electrical energy into mechanical motion for various applications. Figure 1 illustrates the detailed architecture of the PMSM used in our study, showing the integral components, including the rotor, stator, and water jacket; the red area denotes the shrink-fit and press-fit contact, and the components make said fit, which are the water jacket and the stator in the left side and for the right side the housing and stator.

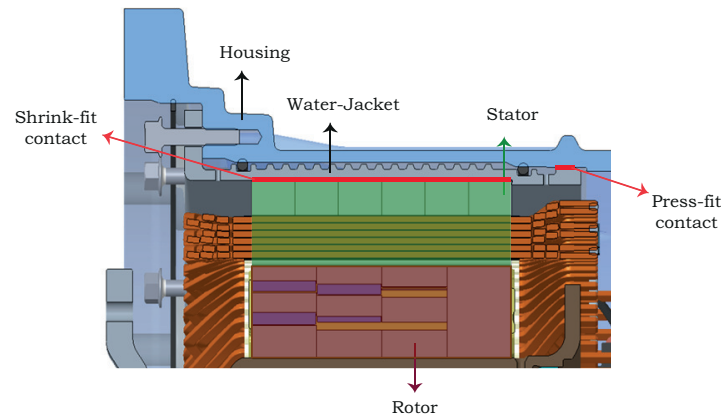


Figure 1. The permanent magnet synchronous motor (PMSM) architecture used in this research.

1.2. Importance and Justification of the Study

One of the most critical aspects of PMSM performance is torque capacity, which directly influences the motor's suitability for demanding applications such as electric vehicles, wind turbines, and industrial automation systems. The torque capacity is significantly affected by the shrink-fit process used in the motor assemblies, where precise interference fits between components like the water jacket and the stator are crucial for maintaining mechanical integrity and efficient thermal conduction. Temperature variations can alter the interference fit, thereby affecting the torque capacity and overall performance of the motor. Understanding how torque capacity varies with temperature in shrink-fit junctions is essential for optimizing motor design and ensuring reliable performance across a wide range of operating conditions. This research is justified by its aim to provide critical insights into these variations, thereby contributing to the development of more reliable and efficient PMSMs for various high-performance applications.

The proposed improvement focuses on enhancing the torque capacity and thermal stability of permanent magnet synchronous motors (PMSMs) through optimized design modifications. This research investigates the influence of temperature variations on shrink-fit junctions between the water jacket and the stator, analyzing torque capacities across a temperature range from $-40\text{ }^{\circ}\text{C}$ to $120\text{ }^{\circ}\text{C}$. By increasing the interference fit in the shrink-fit process and reducing the interference in the press-fit contact, the improved design demonstrates significant performance enhancements.

The remainder of this paper is structured as follows: Section 2 discusses the materials and methods used. Section 3 presents the results of our simulations, offering quantitative insights into the improvements achieved through our design modifications. Section 4 engages in a thorough discussion of these results, evaluating the practical implications and limitations of our study. Finally, we conclude with a summary of our findings and propose future research directions to enhance the performance PMSMs further.

2. Mechanical Design

Electric motors are produced in various types and configurations. Typically, an electric motor has several parts, including a stator, a rotor, a shaft, bearings, and housing that supports and encloses the components. In addition to these primary motor components, some motors may also include electronic components and, in the latest motors, developments commonly known as e-axes (electric axes) are integrated transmission units

that combine the electric motor, transmission, and power electronics into a single compact assembly. These units are designed to be installed directly onto the axle of an electric vehicle, providing an efficient and streamlined solution for electric propulsion.

Understanding motor design characteristics is crucial in the motor design and manufacturing processes. To select appropriate motors for specific applications, these design characteristics must be thoroughly understood.

In the selection of materials for the construction and enhancement of permanent magnet synchronous motors (PMSMs), it is essential to adhere to established standards that ensure quality, durability, and performance. The materials used in our PMSM design, specifically, those for the stator and rotor components, comply with the ASTM International standards, which provide guidelines for material properties such as thermal conductivity, magnetic permeability, and structural integrity. For example, ASTM A276 [25] (Standard Specification for Stainless Steel Bars and Shapes) is crucial for determining the mechanical properties required for the motor's structural components that are subjected to high stresses and temperatures [26]. Furthermore, ASTM A801 (Standard Specification for Wrought Iron-Cobalt High Magnetic Saturation Alloys for Magnetic Components) is utilized to select magnetic materials that offer high magnetic saturation and resistance to demagnetization, a critical factor for the efficiency of PMSMs under various operational conditions [27].

The mechanical design of high-performance electric motors such as PMSMs involves intricate consideration of not only the material properties but also the geometrical and structural aspects of the motor components to optimize their performance and reliability. Key design considerations include the dimensional accuracy of the motor shaft, the alignment and tolerance of the bearings, and the robustness of the assembly to withstand the operational stresses and thermal expansion. The application of these principles ensures each component can handle the specified loads without failure [28].

2.1. Basic Requirements

There are basic requirements that are taken into account when designing an electric motor that in its configuration has shrink-fit between components. This is commonly found between the water jacket and the stator laminations, and between the rotor and the shaft or stator holder. These requirements focus on guaranteeing adequate operation under certain conditions, in which the following points are analyzed.

- Interference fit: Ensure the components are tightly joined without excessive deformation or stress, which is crucial for a strong connection.
- Material compatibility: Choose materials compatible with each other to prevent corrosion and ensure a reliable bond, considering similar thermal expansion coefficients to minimize differential expansion.
- Surface finish: Properly finish mating surfaces to ensure good contact and load distribution, reducing stress concentrations.
- Torque capacity: Determine the torque capacity needed for the joint to withstand mechanical loads without failure.
- Temperature control: Control temperature during assembly to prevent thermal stresses that could lead to premature failure.
- Load distribution: Design for uniform load distribution across the joint to prevent localized stress concentrations.
- Assembly accuracy: Ensure precision machining and assembly for the desired interference fit and joint integrity.
- Prevention of galling: Take measures to prevent friction-induced galling, such as applying lubricants or coatings.

2.2. Motor Torque

Torque is a measurement of the turning force acting on an object to cause that object to rotate or twist about an axis or pivot. Torque, like work, is measured in newton-meters [Nm] in the International System of Units [SI system] or pound-foot [lb f-ft] in the English system.

In the design of electric vehicles (EVs), torque capacity is paramount as it directly affects performance, efficiency, and the driving experience. High torque enables swift acceleration, essential for safety and driver satisfaction, while also facilitating hill climbing and towing capabilities. Moreover, adequate torque capacity enhances regenerative braking efficiency, extending the vehicle's range and optimizing energy usage. Efficiency is optimized when power and torque are balanced, ensuring the motor operates effectively across various driving conditions. Additionally, a motor with a flat torque curve provides smoother acceleration, enhancing driveability. Thus, torque capacity is a critical consideration in EV design, impacting not only performance but also range, efficiency, and overall consumer appeal.

The torque which can be transmitted between cylindrical components by an interference fit can be estimated by

$$T = 2fp\pi b^2L \quad (1)$$

where: T is the torque [N/m]; f , coefficient of friction; p , interference pressure [N/m²]; b , interface radius [m]; and L , length of interference fit [m].

The torque referred to in our study is measured at the junction between the water jacket and the stator, which is critical for understanding the mechanical stress and operational capacity of the motor. This torque measurement is indicative of the forces the motor shaft must withstand. The electromagnetic torque, which is a primary quantity in motor performance analysis, is considered in our simulations as the initial input. This torque generated by the rotor's magnetic field is crucial for setting the operational parameters and is used to assess the mechanical integrity of the stator and water jacket under realistic operational stresses, providing a direct correlation to the shaft's mechanical requirements and ensuring the motor's structural integrity under load.

For electric motors the electromagnetic fields generated between rotor and stator induce angular movement, which generates tangential forces or torque as a output response. This torque is transferred directly to the assembly points where components are fixed. In this work, the torque generated by the PMSM under the velocity operation profile is transferred toward the shrink-fit joint between the water jacket and stator.

The electromagnetic analysis that describes the PMSM performance is shown in Figure 2, where the torque is a function of the velocity profile. For this analysis, the input torque values at 550 V are 400–600 N/m. However, the hold torque goal occurs at peak operation at 650 V, where the torque reaches around 1000 N/m.

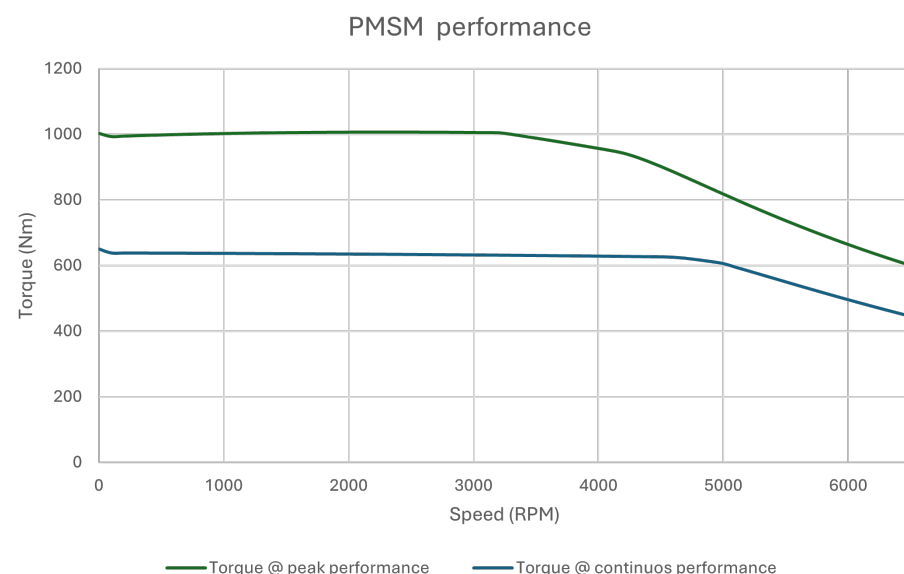


Figure 2. Simulated permanent magnet synchronous motor (PMSM) initial peak and continuous performance.

2.3. Component Tolerances

Control of dimensions is necessary to ensure assembly and interchangeability of components. Tolerances are specified on critical dimensions that affect clearances and interference fits. One method of specifying tolerances is to state the nominal dimension followed by the permissible variation.

2.3.1. Interference Fits

Interference fits are those for which, before assembly, the inside component is larger than the outside component. There is some deformation of the components after assembly and a pressure exists at the mating surfaces. Due to the materials being different, the pressure is given by

$$\rho = \frac{\delta}{2b \frac{1}{E_o} \frac{c^2+b^2}{c^2-b^2} + \mu_o + \frac{1}{E_i} \frac{b^2+a^2}{b^2-a^2} - \mu_i} \quad (2)$$

where ρ is the pressure at the mating surface [N/m²]; δ , total diametral interference (m); a , is the internal radius of the inner cylinder [m]; b , the outer radius of the inner cylinder [m]; c , the outer radius of the outer cylinder [m]; E , Young's modulus [N/m²]; and μ , Poisson's ratio. The subscriptions i and o refer to the inner and outer components, respectively; see Figure 3 where a is the inner diameter of the inner component, b is the outer diameter of the outer component and c is the outer diameter of the outer component.

The tensile stress in the outer component, σ_o , can be calculated from Equation (3) and the compressive stress in the inner component, σ_i , from Equation (4).

$$\sigma_o = \rho \frac{\downarrow c^2 + b^2}{\rightarrow c^2 - b^2} \quad (3)$$

$$\sigma_i = \rho \frac{\downarrow b^2 + a^2}{\rightarrow b^2 - a^2} \quad (4)$$

The increase in the diameter of the outer component, δ_o , due to the tensile stress can be calculated from Equation (5) and the decrease in diameter of the inner component due to the compressive stress, δ_i , from Equation (6).

$$\delta_o = \frac{2bp}{E_o} \frac{\downarrow c^2 + b^2}{\rightarrow c^2 - b^2} + \mu_o \quad (5)$$

$$\delta_i = \frac{2bp}{E_i} \frac{\downarrow b^2 + a^2}{\rightarrow b^2 - a^2} + \mu_i \quad (6)$$

Our study's formula for calculating torque is adapted from *Mechanical Design* by Peter Childs [29]. These equations are utilized to estimate the force exerted on the walls of the water jacket and stator, providing a basis for assessing the mechanical stress and torque capabilities of the assembly. This adaptation allows us to specifically analyze the interactions at the motor's critical junction points.

2.3.2. Least and Maximum Material Conditions

The maximum material condition (MMC) and the least material condition (LMC) are terms used in geometric dimensioning and tolerancing (GDT) to define the extreme conditions of a part's feature within the specified tolerance zone.

Maximum material condition (MMC): This refers to the condition of a feature of size when it contains the maximum amount of material, meaning the feature size is at its largest limit within the specified tolerance zone. In other words, the part is at its upper limit of material condition. For example, for a hole, the MMC would mean the hole is at its smallest diameter within the tolerance zone, while for a shaft, the MMC would mean the shaft is at its largest diameter within the tolerance zone. MMC is often used to ensure proper fit

and functionality of mating parts, especially in assembly applications where a clearance or interference fit is critical [29].

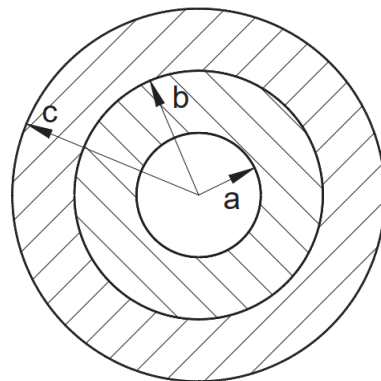


Figure 3. Terminology for cylindrical interference fit.

Least material condition (LMC): Conversely, LMC refers to the condition of a feature of size when it contains the least amount of material, meaning the feature size is at its smallest limit within the specified tolerance zone. In other words, the part is at its lower limit of material condition. For example, for a hole, the LMC would mean the hole is at its largest diameter within the tolerance zone, while for a shaft, the LMC would mean the shaft is at its smallest diameter within the tolerance zone. LMC is often used to ensure proper assembly and functionality of parts with a clearance fit, where the minimum material condition ensures the maximum clearance [29]. The Figure 4 shows how the stator and the water jacket are described, describing the interior and exterior diameters of each one.

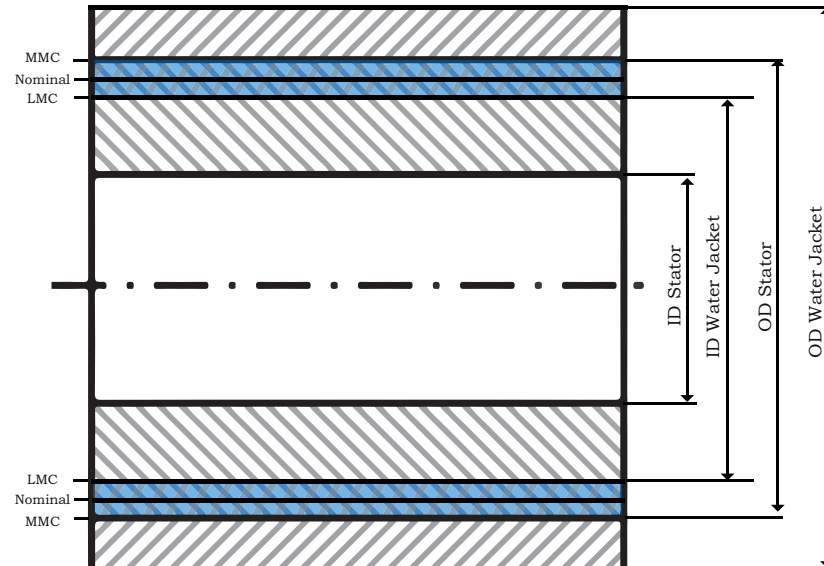


Figure 4. Interference description: shaft and hub.

2.3.3. Shrink-Fit Process and ISO Fits

Shrink-fit is a semi-permanent assembly system used extensively in various industries due to its ability to transmit large torques through high contact pressure at the interface of mating components. This method offers several advantages over press-fit: it minimizes mechanical stresses and deformation of the rotor core, allows for symmetrical shrinking of the rotor core onto a shaft, requires less surface finishing, and is completely controllable.

Shrink-fit techniques leverage the thermal expansion and contraction properties of materials during machine assembly processes. The coefficient of linear thermal expansion,

which measures how much a material expands with a temperature change, is crucial in this context. It defines the linear dimension change per unit temperature change.

The basic use of an electric motor is for high-torque demands and based on the interference fits and considering the required torque, the defined setting is U7/h6 based on the ISO 286-1:2010 standard [30], and taking into account that the stator (shaft) will be used as a basis for defining the hole (water jacket) and its respective tolerances.

For the definition of the tolerances and the internal diameter of the water jacket, the external diameter of the stator is considered as the shaft basis, where, with a nominal diameter of 355.023 mm, the tolerances of the hole are defined as U7 and the shaft tolerances of h6 are defined, resulting in the hole having a maximum size of 354.654 mm, and a minimum size of 354.597 mm; with this, the background in the development of this research on the baseline definition the specific diameters and tolerances used is shown.

2.3.4. Torque Transmission through Mechanical Joints (Shrink-Fit)

When considering torque capacity in components utilizing a shrink-fit process as a mechanical joint, several factors come into play to ensure the joint's integrity and reliability under load. In a shrink-fit assembly, such as coupling a hub to a shaft, the torque capacity primarily depends on the strength and material properties of both the hub and the shaft, as well as the effectiveness of the shrink-fit process itself.

The torque capacity of a shrink-fit joint relies on material selection, where both hub and shaft must offer sufficient strength, typically utilizing steel alloys for high-torque applications. Achieving an appropriate interference fit, and balancing tightness with assembly concerns directly impacts torque capacity. A proper surface finish on mating surfaces is crucial to maximizing contact area and torque transmission. Controlled temperature gradients during assembly prevent thermal stress that could compromise joint integrity. Additionally, design for uniform load distribution across the interface helps prevent localized stress concentrations and premature failure.

The free-body diagram and description of the forces and moments produced by the shrink-fit and press-fit are shown in Figure 5 based on [28]; this diagram helps to analyze the distribution and how improvements could be applied for a good result; $F_{support}$ represents the preload on bolted joints, this is considered as mechanical fixing between the water jacket and housing; F_{stator} is the reaction force of the stator, and $F_{housing}$ is the force that the housing applies to the water jacket. The loads considered come from the thermal effects by temperature changes, the torque generated by electromagnetic forces, and expansion by the pressure joint (press-fit) and shrink-fit.

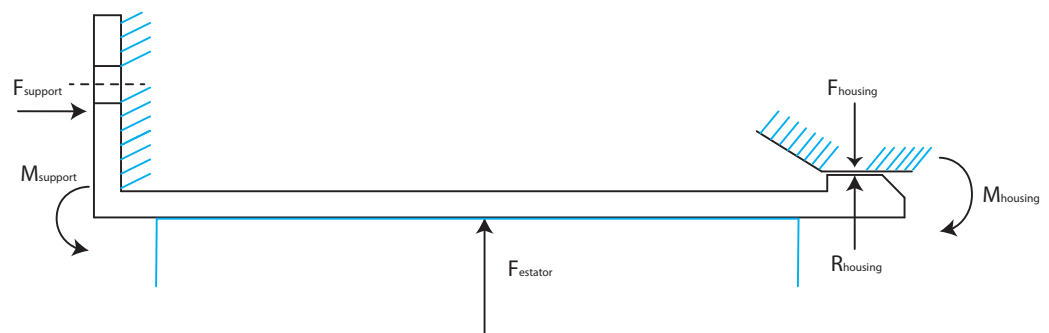


Figure 5. Free-body diagram of water jacket.

2.4. Operating Temperatures

In a generator or electric motor, the operating temperature points depend on various factors such as the design, materials used, and intended application. Generally, the environment temperature range ($-40\text{ }^{\circ}\text{C}$ to $120\text{ }^{\circ}\text{C}$) provides the context for determining safe operating temperatures.

For a synchronous permanent magnet motor, the maximum temperature typically occurs at the stator winding and the rotor surface, where electrical losses and magnetic flux

concentration are most pronounced. The gradient of temperature decrease from the rotor to the housing varies depending on factors like insulation, cooling mechanisms, and thermal conductivity of materials. Typically, the rotor experiences higher temperatures due to its proximity to the magnetic field and electrical currents. At the same time, the housing may have a lower temperature due to heat dissipation through conduction and possibly cooling mechanisms such as fans or liquid cooling systems. The gradient may vary, but generally, the temperature decreases from the rotor towards the housing, with the specific profile influenced by the motor's design and operating conditions. Figure 6 shows the temperature between the water jacket and the stator.

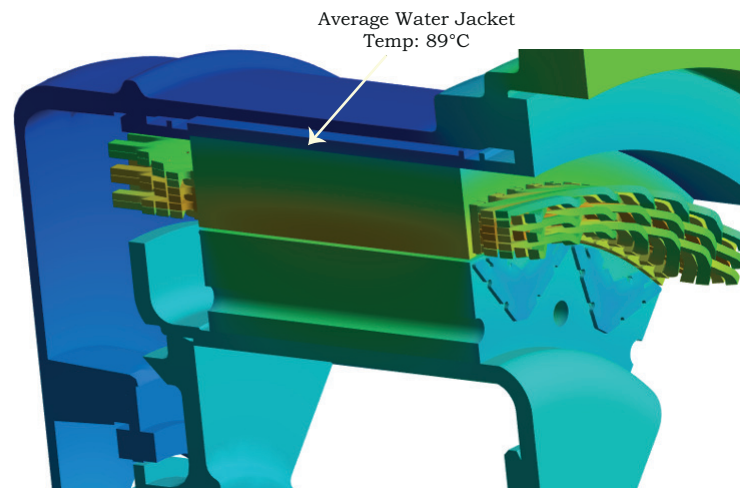


Figure 6. Temperature gradient in the e-motor analyzed.

2.5. Thermal Management

Thermal management in synchronous permanent magnet electric motors is crucial for ensuring optimal performance, efficiency, and reliability while preventing overheating and potential damage to the motor components. Several strategies are commonly employed for effective thermal management and the temperatures involved and analyzed are the rotor's electromagnetic temperature effects and the thermal output due to current flow through the stator's hairpins. These factors critically influence the thermal management strategies and material selection for the motor, as the heat distribution affects the overall efficiency and performance durability.

Water jackets involve circulating coolant (typically water or a water–glycol mixture) through channels or jackets integrated within the motor housing to dissipate heat effectively. This method offers efficient cooling by directly contacting motor components, particularly the stator windings and rotor, where heat generation is significant. The water jacket system regulates temperature by absorbing heat from these components and transferring it away, maintaining optimal operating conditions and preventing overheating.

2.6. Software Used

The simulations were carried out in Ansys Mechanical 2022 R2, with geometric interference fit effects in frictional contacts and thermal conditions. For the frictional contact the formulation is given as follows.

Friction coefficient: A non-zero value will activate Coulomb-type friction between bodies $F = \mu R$. The relative velocity $[v]$ of sliding interfaces can influence frictional forces. A dynamic frictional formulation for the coefficient of friction can be used.

$$\mu = \mu_d + (\mu_s - \mu_d)e^{-\beta v} \quad (7)$$

where μ_s is the friction coefficient, μ_d is the dynamic coefficient of friction, β is the exponential decay coefficient, and v is the relative sliding velocity at point contact; non-zero values of the dynamic coefficient and decay constant were used.

And, for the thermal effects the expansion coefficient used is

$$\varepsilon^{th} = a^{se}(t)(T - T_{ref}) \quad (8)$$

where $a^{se}(t)$ is the temperature-dependent secant coefficient of thermal expansion; $a^{se}(t)$ is input in one of three ways:

- Input $a^{se}(t)$ directly;
- Computed using Equation (9) from $a^{in}(T)$, the instantaneous coefficients of thermal expansion:

$$a^{se}(T) = \frac{\int_{T_{ref}}^T a^{in}(T)dT}{T - T_{ref}} \quad (9)$$

- Computed using Equation (10) from $\varepsilon^{ith}(T)$, the input thermal strains:

$$a^{se}(T) = \frac{\varepsilon^{ith}(T)}{T - T_{ref}} \quad (10)$$

$a^{se}(T)$ is computed from ε^{ith} by rearranging Equation (8) and ε^{th} (thermal strain) is related to $a^{in}(T)$ by

$$\varepsilon^{th}(T) = \int_{T_{ref}}^T a^{in}(T)dT \quad (11)$$

These equations use the software to converge to a solution.

3. Results and Discussion

The maximum and minimum tolerances define the interferences that may exist in the analyzed components, and by adding the temperatures, four cases are considered for analysis:

- MMC condition at -40 °C;
- MMC condition at 120 °C;
- LMC condition at -40 °C;
- LMC condition at 120 °C.

These can be considered as the worst cases, where the material can be the minimum or maximum and where the temperature is the maximum or the minimum. Therefore, the results obtained will give high reliability concerning the requirements that there may be when a motor is being designed concerning the torque that it is capable of being delivered as well as the maximum effort that can be resisted depending on the temperature.

3.1. Baseline Definition

The initial analysis is carried out based on the following tolerances and the diametric interference was found in the water jacket and the stator. The housing and the stator are also considered since, by design, there is also a contact.

Table 1 shows the nominal diameters and their respective tolerances in the water jacket, stator, and housing and their respective values when MMC and LMC are considered. The nominal interference on the shrink-fit is 0.398 mm, and the value is less when the LMC is analyzed, with a value of 0.347, and when the MMC is analyzed, the value of the diametrical interference is 0.449, higher than the nominal. It is the same for the press-fit contact, the nominal value being in the middle of the LMC and MMC.

The definition of interference at nominal, minimum, and maximum helps us to know the ranges in which the electric motor can deliver the torque; in the same way, we can analyze the stress that is found in the material when it is cooled or heated and the deflection due to the stress it produces in the material.

Table 1. Tolerances and diametral interference baseline design.

Shrink-fit contact (water jacket and stator)				
Component	LMC	MMC	TOL±	Nominal
Water jacket inner diameter (ID)	354.653	354.597	0.028	354.625
Stator outer diameter (OD)	355	355.046	0.023	355.023
Diametral interference	0.347	0.449	0.051	0.398
Press-fit contact (housing and water jacket)				
Water jacket OD	354.185	354.215	0.015	354.2
Housing ID	354.15	354.05	0.05	354.1
Diametral interference	0.035	0.165	0.065	0.1

The baseline design based on specific tolerances and diametric interferences serves as a reference point for further analysis and comparison. This approach allows for a structured assessment of how design modifications impact the torque capacity and thermal stability under varying conditions.

3.1.1. Baseline Stress Analysis

After defining the interferences, the stresses that occur in the material can be analyzed; these stresses help define the deflection of the component.

In our analysis of the stress results, we have meticulously documented the baseline von Mises stress results for both LMC and MMC conditions at $-40\text{ }^{\circ}\text{C}$ and $120\text{ }^{\circ}\text{C}$. Table 2 analyzes the main stress and the equivalent stress. These results were obtained for the supports that the housing has and the loads that represent the torque and the forces that are produced are considered, thus the maximum stresses. They are found in the MMC condition at $-40\text{ }^{\circ}\text{C}$, with a value of 230.32 MPa compared to the condition, but at $120\text{ }^{\circ}\text{C}$ the stress is less, with a value of 101.41 MPa, showing that when there are low temperatures the material tends to contract, and when the temperature rises, the material tends to expand, reducing the stresses on the material. This stress can be compared with the yield strength of the material, and the main objective is to keep the stress below the yield strength. If the elastic limit of the material is exceeded, the plasticity of the material must be analyzed in an acceptable range with extra analysis, ensuring that the plasticity does not exceed 1% in the final elongation of the material.

Table 2. Baseline von Mises stress results for LMC and MMC at $-40\text{ }^{\circ}\text{C}$ and $120\text{ }^{\circ}\text{C}$.

	MMC at $-40\text{ }^{\circ}\text{C}$		MMC at $120\text{ }^{\circ}\text{C}$		LMC at $-40\text{ }^{\circ}\text{C}$		LMC at $120\text{ }^{\circ}\text{C}$	
	Max [MPa]	Min [MPa]						
Principal Stress	230.32	-30.091	101.41	-34.19	190.7	-28.05	102.36	-31.37
Equivalent Stress	195.63	0.5983	151.62	0.028	151.72	0.547	134.88	0.017

Figure 7a shows the stress when the boundary condition is set at $-40\text{ }^{\circ}\text{C}$ around the material in the water jacket; the orange zone is the smooth surface; this zone has the maximum stress due to the direct contact of the shrink-fit with the stator; at the edges the stress is less in this analysis; there exists a contraction due to the cold, in this condition the stresses in the MMC and LMC are higher. Whereas when analyzed at $120\text{ }^{\circ}\text{C}$ the stress drops considerably as the material expands. Therefore, the stress found in the material tends to be lower in the LMC and MMC; see Figure 7b.

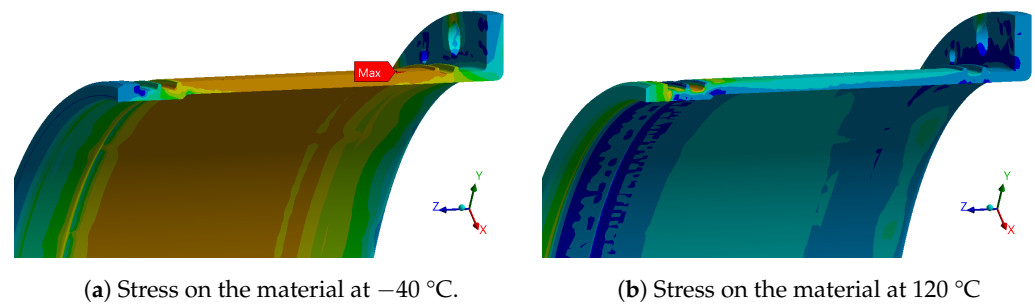


Figure 7. Stress on the material due to the temperature at $-40\text{ }^{\circ}\text{C}$ and $120\text{ }^{\circ}\text{C}$.

3.1.2. Baseline Deflection Analysis

The 2D radial deflection is shown in Figure 8, which offers a magnified view of the expansion and contraction processes within the motor's assembly, showing the physical changes under thermal stress at a 50-times magnification. This visual representation is critical for understanding the dynamic behavior of the motor components under operational temperature variations, which significantly influence mechanical fit and performance stability.

Contraction analysis: The contraction view depicted in Figure 8a illustrates how components react when subjected to lower temperatures. As temperatures decrease, materials contract, leading to increased mechanical interference between the water jacket and the stator. This condition can enhance the torque transmission efficiency due to tighter fits but may also elevate the stress levels within the materials, posing risks of fatigue over prolonged use.

Expansion analysis: Conversely, the expansion view in Figure 8b reveals the behavior of these components under elevated temperatures. As the material expands, the interference fit decreases, potentially leading to slippage or reduced torque capability. The visual data clearly show how expansion can alter the contact surfaces between components, emphasizing the need for robust thermal management to maintain operational integrity.

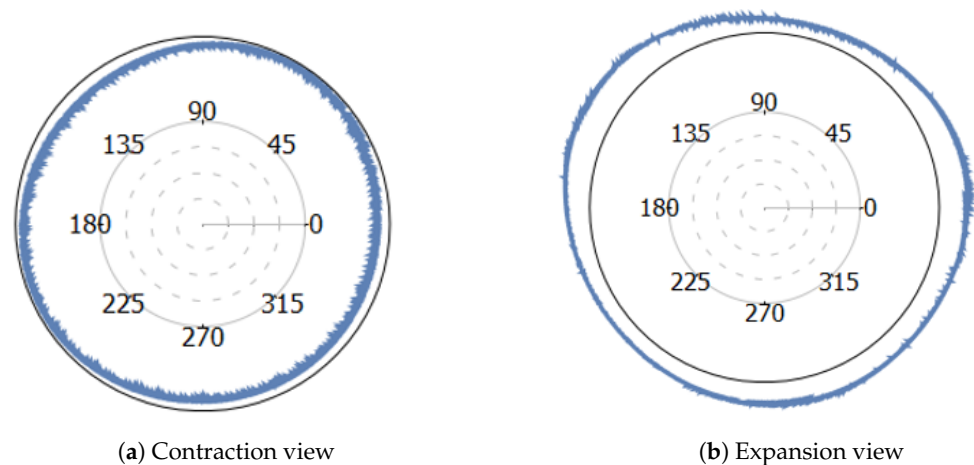


Figure 8. Expansion and contraction; view magnified 50 times.

The graphical representations of deflection in the water jacket and the stator effectively highlight areas of varying stress concentrations through a color-coded gradient from green to red. In the water jacket, Figure 9a, the most pronounced deflection is visibly concentrated in the central section, indicated by the bright red color. This central deflection suggests a significant response to external pressures or temperature variations, which are likely more intense in this middle area. The gradual change in color towards the edges—transitioning from yellow to green—indicates decreasing deflection, suggesting these peripheral regions are either structurally more robust or subjected to less stress. The analysis of this pattern is crucial as it helps identify potential weak points that could be prone to mechanical failures

or operational inefficiencies, especially in scenarios where this component interfaces tightly with others.

Similarly, the stator shown in Figure 9b presents a cylindrical visualization of deflection, with the greatest deformation highlighted in red at the center of its curvature. This pattern suggests that the midpoint of the stator's curve is subjected to the highest stress during operation, which could be due to mechanical loads or thermal expansions. The edges of the stator, depicted in green, experience the least deflection, indicating lower stress levels and potentially higher structural integrity in these regions.

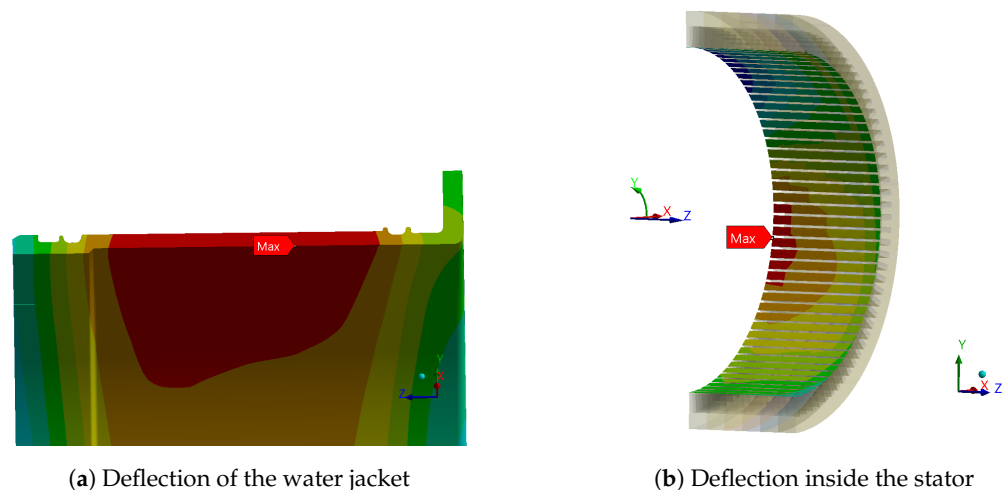


Figure 9. Deflection of the material components.

The deflection of the water jacket due to temperature changes can be analyzed by thermal expansion or contraction. When the temperature increases, its material expands, causing it to deform. Similarly, when the temperature decreases, the material contracts, leading to deformation in the opposite direction.

Table 3 shows the results; the water jacket deflection is analyzed at six heights due to the applied loads being different; the water jacket is not balanced in its constitution. In the same way, the water jacket can show a variation in the circularity itself once the water jacket contracts or expands with stress.

The data reveal interesting trends in the radial deflection behavior of materials under varying thermal conditions and constraints (MMC and LMC). At $-40\text{ }^{\circ}\text{C}$, observed through MMC, all samples contract, with S6 showing the most significant contraction at -0.106 mm , highlighting its sensitivity to cold temperatures. Conversely, S1 exhibits the least contraction at -0.067 mm , suggesting it is less prone to shrinkage under these conditions. Under the LMC at the same temperature the pattern remains similar, with S6 again demonstrating the greatest contraction (-0.235 mm), and S1 showing minimal change from its MMC state (-0.063 mm). This consistency in each sample's response under different material conditions underscores their inherent material properties and behavior under cold stress.

At $120\text{ }^{\circ}\text{C}$, the behavior shifts noticeably, particularly under LMC, where all samples expand. In this warmer environment, S1 and S2 exhibit the smallest expansions at 0.322 mm and 0.300 mm , respectively, under MMC, which might suggest that their composition or structure is less reactive to heat-induced expansion compared to others. Remarkably, under LMC, all samples show positive deflections (expansion), with S1 again showing the least at 0.322 mm , and S6, despite its significant contractions at colder temperatures, expanding to 0.287 mm . This different response at higher temperatures indicates that the materials can recover or even exceed their original dimensions, impacting their circularity and possibly affecting mechanical integrity in practical applications, where precise dimensional stability is crucial.

Table 3. Baseline radial deflection analysis.

	Deflection MMC/−40 °C		Deflection MMC/120 °C		Deflection LMC/−40 °C		Deflection LMC/120 °C	
	Δr_{max} [mm]	Δr_{min} [mm]						
S1	−0.067	−0.288	0.314	−0.029	−0.063	−0.0269	0.322	−0.029
S2	−0.071	−0.205	0.31	0.033	−0.067	−0.196	0.3	0.037
S3	−0.077	−0.193	0.305	0.045	−0.073	−0.185	0.291	0.067
S4	−0.088	−0.189	0.307	0.042	−0.084	−0.181	0.289	0.065
S5	−0.094	−0.187	0.311	0.037	−0.088	−0.178	0.288	0.061
S6	−0.106	−0.263	0.31	0.013	−0.1	−0.235	0.287	0.054

3.2. Design Improvement

The torque capacity can be improved by increasing the interference between the water jacket and the stator, but also the stresses tend to increase, which is why for the torque capacity improvement stage, an increase in the shrink-fit and a reduction in interference in the press-fit is considered.

Table 4 shows that with the new inner diameter of the water jacket and keeping the same outer diameter of the stator, the nominal interference is now 0.423 mm, while previously it was 0.398 mm, where the increase in interference is 6.28%. In the same way, the values of LMC and MMC changed, where diametric interference in the LMC is 0.38 mm and diametric interference in the MMC is 0.466 mm.

In the press-fit, on the other hand, the interference between the water jacket and the housing is reduced to release the stress that is concentrated in the water jacket. If the interference is increased, the F_{stator} that is applied will be greater, and the reaction force of the material will also increase, but by reducing the $F_{housing}$ we will be reducing the torsional moment that occurs in $M_{housing}$, as shown in Figure 5.

Table 4. Tolerances and diametral interference of improved design.

Shrink-fit contact (water jacket and stator)				
Component	LMC	MMC	TOL±	Nominal
Water jacket inner diameter (ID)	354.62	354.58	0.02	354.6
Stator outer diameter (OD)	355	355.046	0.023	355.023
Diametral interference	0.38	0.466	0.043	0.423
Press-fit contact (housing and water jacket)				
Water jacket OD	354.185	354.215	0.02	354.15
Housing ID	354.15	354.05	0.02	354.1
Diametral interference	0.01	0.09	0.04	0.05

3.2.1. Improved Design's Stress Analysis

The stress analysis, as well as at baseline, is analyzed for four different cases, taking into account that the interference increased in the shrink-fit and the interference decreased in the press-fit; the values found are described in Table 5. If we compare the data obtained in the MMC at −40 °C, the principal maximum stress found in the water jacket is 207.87 MPa, and if this is compared with the baseline, there is a stress reduction of 9.74%. And, if the equivalent stress is analyzed, the reduction is 6.70%, going from 196.63 MPa to 182.51 MPa. When the MMC at 120 °C is analyzed, there is an increase in stress in this specific case; the main stress rose from 101.41 MPa to 148.51 MPa, which represents 31.17%. If the equivalent stress is analyzed, the increase is 1.44%. For LMC cases, something similar

happens at $-40\text{ }^{\circ}\text{C}$, the values of the main stress are reduced while in the equivalent stress they increase slightly.

Table 5. Improved design's von Mises stress results in LMC and MMC at $-40\text{ }^{\circ}\text{C}$ and $120\text{ }^{\circ}\text{C}$.

	MMC at $-40\text{ }^{\circ}\text{C}$		MMC at $120\text{ }^{\circ}\text{C}$		LMC at $-40\text{ }^{\circ}\text{C}$		LMC at $120\text{ }^{\circ}\text{C}$	
	Max [MPa]	Min [MPa]						
Principal Stress	207.87	-35.905	148.51	-33.64	181.69	-34.19	135	-30.37
Equivalent Stress	182.51	0.8845	153.84	0.12	154.72	0.75	142.28	0.07

3.2.2. Improved Design's Deflection Analysis

Table 6 shows the deflection results after improving the interferences, where at $-40\text{ }^{\circ}\text{C}$, under both MMC and LMC conditions all samples exhibit contraction (negative values), but it is notable that the maximum contraction values are less severe compared to the baseline design. For instance, under MMC, the greatest contraction observed is -0.072 mm in sample S6, a slight improvement over the baseline's most extreme contraction. The minimum deflection values under LMC also show slight improvements, with the least contraction being less pronounced than in the baseline data, suggesting enhanced resistance to thermal contraction at lower temperatures. This improved consistency in contraction across the samples might indicate a more uniform material distribution or enhanced structural integrity in the new design.

At $120\text{ }^{\circ}\text{C}$, the deflection shifts towards expansion in many samples, which is expected with increased temperatures. Under MMC, the expansions are modest but positive for most samples, demonstrating a controlled response to thermal expansion. For example, sample S1 expands by 0.329 mm at its maximum, showing a stable and predictable expansion. Under LMC, sample S1 again shows the largest expansion at 0.342 mm , reflecting a design that can accommodate thermal stresses more uniformly. The minimum deflection values are significantly improved compared to the baseline, with even the minimal expansions and contractions remaining close to zero, suggesting that the improved design maintains its dimensions better under varying temperatures.

Table 6. Improved design's radial deflection analysis.

	Deflection MMC/ $-40\text{ }^{\circ}\text{C}$		Deflection MMC/ $120\text{ }^{\circ}\text{C}$		Deflection LMC/ $-40\text{ }^{\circ}\text{C}$		Deflection LMC/ $120\text{ }^{\circ}\text{C}$	
	Δr_{max} [mm]	Δr_{min} [mm]						
S1	-0.053	-0.287	0.329	-0.05	-0.051	-0.272	0.342	-0.045
S2	-0.053	-0.205	0.303	0.016	-0.051	-0.199	0.3	0.02
S3	-0.055	-0.198	0.277	0.037	-0.053	-0.192	0.27	0.047
S4	-0.059	-0.198	0.257	0.035	-0.056	-0.192	0.251	0.043
S5	-0.06	-0.2	0.254	0.033	-0.057	-0.194	0.255	0.041
S6	-0.072	-0.273	0.251	-0.019	-0.068	-0.235	0.252	0.004

3.3. Torque Capacity

The torques obtained from the simulations are directly related to interference and temperature, so for this analysis, several temperatures are considered, starting from $-40\text{ }^{\circ}\text{C}$, which is the coldest temperature at which the e-motor should operate, to $22\text{ }^{\circ}\text{C}$, which represents an ambient temperature, to $90\text{ }^{\circ}\text{C}$, which represents an approximate operating temperature between the water jacket and the stator defined by the simulation, and to $110\text{ }^{\circ}\text{C}$ and $120\text{ }^{\circ}\text{C}$, which would be cases where the temperature is much higher than the operating temperature, considered as extreme cases of high temperatures.

Table 7 shows the torque with the baseline interference and tolerances, where at 120 °C and because the material expands, the torques in LMC, nominal, and MMC are lower than the rest of the cases, where the minimum value is 549 Nm and the maximum torque is 9032 Nm in MMC at −40 °C, a condition where there is the greatest amount of material and with the cold the material tends to generate greater interference.

Table 7. Baseline design's torque capacity.

Temperature	Torque LMC [Nm]	Torque Nominal [Nm]	Torque MMC [Nm]
−40 °C	7648	8297	9032
22 °C	4828	5524	6283
90 °C	1596	2020	2455
110 °C	815	1337	1864
120 °C	549	1015	1533

Meanwhile, Table 8 analyzes the same temperature levels, but the values obtained are higher. For the LMC at 120 °C, the torque is 842 Nm. If compared to the baseline, this is an increase of 55.38%, and when analyzed in MMC at −40 °C the increase is 2.38%, with a final torque obtained of 9247. The variation in these values lies in the increase in interference and the reduction in the tolerances.

Table 8. Improved design's torque capacity.

Temperature	Torque LMC [Nm]	Torque Nominal [Nm]	Torque MMC [Nm]
−40 °C	8055	8657	9247
22 °C	5274	5883	6493
90 °C	1812	2305	2822
110 °C	1153	1600	2052
120 °C	842	1274	1618

The study shows that the improved design achieves higher torque capacities, particularly at elevated temperatures, by effectively managing thermal expansion and contraction, thus maintaining mechanical integrity and efficient thermal conduction. These findings underscore the importance of precise design adjustments and material selection in developing PMSMs that can reliably operate under varying thermal conditions, making them suitable for demanding applications such as electric vehicles and industrial automation.

3.4. Validation

To validate the design, a sample was tested in a dynamometer at an ambient temperature; the torque curve, represented by the blue line in Figure 10, shows a rapid increase in torque from 0 to around 1000 RPM, stabilizing at approximately 650 Nm between 1000 and 5000 RPM. Beyond 5000 RPM, the torque decreases slightly, ending just above 450 Nm at 6000 RPM. This indicates that the motor maintains a high and stable torque in the mid-speed range but experiences a performance drop at higher speeds.

The current curve, depicted by the orange line, mirrors this pattern, with a rapid rise to just above 400 Arms at around 1000 RPM. It then remains relatively stable, fluctuating around 550 Arms up to 5000 RPM. The motor operates most efficiently between 1000 and 5000 RPM, where both torque and current are stable.

The torque found in the validation performance is similar in the simulated continuous performance; the torque is around 650 Nm in both cases.

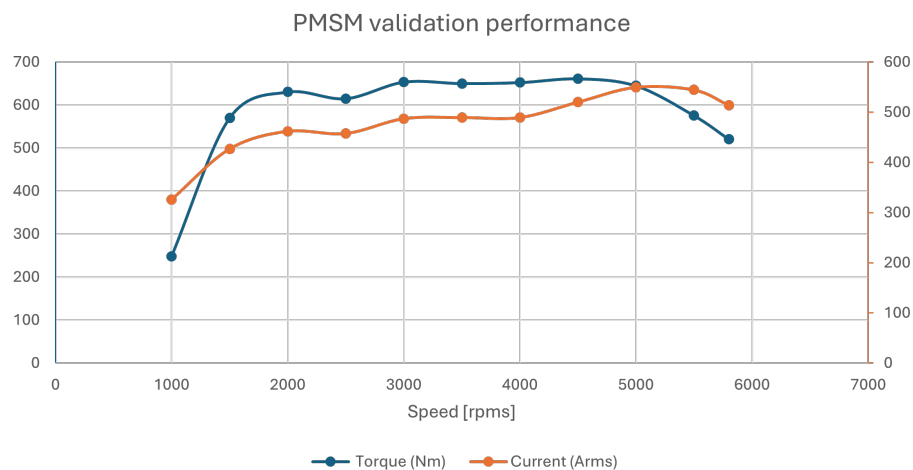


Figure 10. Permanent magnet synchronous motor (PMSM) validation performance.

4. Conclusions

We would like to point out that increasing the interference in the shrink-fit increases the torque capacity. Analyzing the stresses that occur in the material, these were slightly less since the reduction of the press-fit was considered a good way to release tension and reduce the torsional moments presented by the analyzed model.

The comparison of torque capacity data for the baseline and improved designs of the permanent magnet synchronous motor (PMSM) reveals significant performance enhancements in the improved design, particularly at elevated temperatures.

The minimum improvement occurs at $-40\text{ }^{\circ}\text{C}$, where the torque capacity for the LMC rises from 7648 Nm to 8055 Nm, a 5.3% increase, and for MMC, from 9032 Nm to 9247 Nm, a 2.4% increase, indicating a modest improvement in cold conditions.

At $22\text{ }^{\circ}\text{C}$, the torque capacity of the improved design rises from 4828 Nm (LMC) to 5274 Nm (LMC) and from 6263 Nm (MMC) to 6473 Nm (MMC), demonstrating enhanced performance at room temperature. At $90\text{ }^{\circ}\text{C}$, the improved design significantly increases the torque capacity from 1576 Nm (LMC) to 1812 Nm (LMC) and from 2455 Nm (MMC) to 2802 Nm (MMC), showing better thermal stability. At $110\text{ }^{\circ}\text{C}$, the improved design's torque capacity jumps from 815 Nm (LMC) to 1153 Nm (LMC) and from 1864 Nm (MMC) to 2032 Nm (MMC), highlighting substantial improvements at high temperatures.

The maximum improvement is observed at $120\text{ }^{\circ}\text{C}$, where the torque capacity for the least material condition (LMC) increases from 549 Nm to 842 Nm, a 55.4% increase, and for the maximum material condition (MMC) from 1533 Nm to 1618 Nm, a 5.6% increase, demonstrating its superior performance in extreme heat.

The improved design significantly enhances torque capacity across all temperatures compared to the baseline design, with the most notable gains at higher temperatures.

Comparing the torque capacity calculated in the baseline and the improved design with the validation performance shows a safety factor at all temperatures, which demonstrates that our electric motor is capable of working between $-40\text{ }^{\circ}\text{C}$ and $120\text{ }^{\circ}\text{C}$ in the LMC and MMC without concerns.

However, challenges remain in optimizing material properties and cooling techniques to further increase reliability and efficiency. Future studies should focus on exploring alternative materials with higher temperature tolerances and improved magnetic properties. Additionally, integrating advanced cooling systems such as phase-change materials or enhanced liquid cooling solutions could address the thermal management challenges inherent in high-performance motor applications.

Author Contributions: Conceptualization, D.S.P.-B. and L.M.-C.; writing—original draft preparation, D.S.P.-B.; writing—review and editing, L.M.-C. and E.A.L.-C.; visualization, E.A.L.-C.; supervision, L.M.-C. and J.C.J.-M. All authors have read and agreed to the published version of the manuscript.

Funding: This research received no external funding.

Data Availability Statement: The original contributions presented in the study are included in the article, further inquiries can be directed to the corresponding author.

Acknowledgments: We thank the UISEK University in Ecuador, for the valuable collaboration.

Conflicts of Interest: The authors declare no conflicts of interest.

Abbreviations

The following abbreviations are used in this manuscript:

EV	Electric vehicle
ID	Inner diameter
IM	Induction motor
GDT	Geometric dimensioning and tolerancing
LMC	Least material condition
MMC	Maximum material condition
OD	Outer diameter
PMSM	Permanent magnet synchronous motor

References

1. Sakunthala, S.; Kiranmayi, R.; Mandadi, P.N. A study on industrial motor drives: Comparison and applications of PMSM and BLDC motor drives. In Proceedings of the 2017 International Conference on Energy, Communication, Data Analytics and Soft Computing, ICECDS 2017, Chennai, India, 1–2 August 2017; pp. 537–540. [\[CrossRef\]](#)
2. Zhou, Y.; Yan, Z.; Duan, Q.; Wang, L.; Wu, X. Direct torque control strategy of five-phase PMSM with load capacity enhancement. *IET Power Electron.* **2019**, *12*, 598–606. [\[CrossRef\]](#)
3. Hailemariam, Z.M.; Leidhold, R.; Tesfamariam, G.T. Real-Time Speed Control of a PMSM for Wind Turbine Application. In Proceedings of the IEEE PES/IAS PowerAfrica Conference: Power Economics and Energy Innovation in Africa, PowerAfrica 2019, Abuja, Nigeria, 20–23 August 2019; pp. 396–401. [\[CrossRef\]](#)
4. Bilgin, O.; Kazan, F.A. The effect of magnet temperature on speed, current and torque in PMSMs. In Proceedings of the 2016 22nd International Conference on Electrical Machines, ICEM 2016, Lausanne, Switzerland, 4–7 September 2016; pp. 2080–2085. [\[CrossRef\]](#)
5. Ruoho, S.; Kolehmainen, J.; Ikäheimo, J.; Arkkio, A. Interdependence of demagnetization, loading, and temperature rise in a permanent-magnet synchronous motor. *IEEE Trans. Magn.* **2010**, *46*, 949–953. [\[CrossRef\]](#)
6. McMillan, M.D.; Booker, J.D.; Smith, D.J.; Fedorciuc Onisa, C.; Korsunsky, A.M.; Song, X.; Baimpas, N.; Evans, A. Analysis of increasing torque with recurrent slip in interference-fits. *Eng. Fail. Anal.* **2016**, *62*, 58–74. [\[CrossRef\]](#)
7. Dambrauskas, K.; Vanagas, J.; Zimnickas, T.; Kalvaitis, A.; Ažubalis, M. A method for efficiency determination of permanent magnet synchronous motor. *Energies* **2020**, *13*, 1004. [\[CrossRef\]](#)
8. König, P.; Sharma, D.; Konda, K.R.; Xie, T.; Höschler, K. Comprehensive Review on Cooling of Permanent Magnet Synchronous Motors and Their Qualitative Assessment for Aerospace Applications. *Energies* **2023**, *16*, 7524. [\[CrossRef\]](#)
9. Krüger, B.; Keinprecht, G.; Filomeno, G.; Dennin, D.; Tenberge, P. Design and optimisation of single motor electric powertrains considering different transmission topologies. *Mech. Mach. Theory* **2022**, *168*, 104578. [\[CrossRef\]](#)
10. Louback, E.; Biswas, A.; Machado, F.; Emadi, A. A review of the design process of energy management systems for dual-motor battery electric vehicles. *Renew. Sustain. Energy Rev.* **2024**, *193*, 114293. [\[CrossRef\]](#)
11. Nguyen, C.T.; Nguyễn, B.H.; João, J.P.; Ta, M.C. Optimal drivetrain design methodology for enhancing dynamic and energy performances of dual-motor electric vehicles. *Energy Convers. Manag.* **2022**, *252*, 115054. [\[CrossRef\]](#)
12. Pérez-Cardona, J.R.; Deng, S.; Sutherland, J.W. Optimization of a parametric product design using techno-economic assessment and environmental characteristics with application to an electric traction motor. *Resour. Conserv. Recycl.* **2024**, *206*, 107626. [\[CrossRef\]](#)
13. Borsboom, O.; Salazar, M.; Hofman, T. Electric Motor Design Optimization: A Convex Surrogate Modeling Approach. *IFAC-PapersOnLine* **2022**, *55*, 373–378. [\[CrossRef\]](#)
14. Gobbi, M.; Sattar, A.; Palazzetti, R.; Mastinu, G. Traction motors for electric vehicles: Maximization of mechanical efficiency—A review. *Appl. Energy* **2024**, *357*, 122496. [\[CrossRef\]](#)
15. Satrústegui De Legarra, M. *Thermal and Hydraulic Design of Water-Based Cooling Systems for Electrical Machines*; Servicio de Publicaciones: Madrid, Spain, 2017; p. 270.
16. Park, J.; Han, K.; Choi, H.S.; Park, I.S. Cooling and dynamic performance of electric vehicle traction motor adopting direct slot cooling method. *Int. Commun. Heat Mass Transf.* **2023**, *147*, 106970. [\[CrossRef\]](#)
17. Raj, J.A.P.S.; Asirvatham, L.G.; Angeline, A.A.; Manova, S.; Rakshith, B.L.; Bose, J.R.; Mahian, O.; Wongwises, S. Thermal management strategies and power ratings of electric vehicle motors. *Renew. Sustain. Energy Rev.* **2024**, *189*, 113874. [\[CrossRef\]](#)

18. Guo, F.; Chu, Q.; Li, C. Torque analysis and stator windings influence research on negative-salient permanent magnet synchronous motor. *Energy Rep.* **2023**, *9*, 416–424. [[CrossRef](#)]
19. Aktas, M.; Awaili, K.; Ehsani, M.; Arisoy, A. Direct torque control versus indirect field-oriented control of induction motors for electric vehicle applications. *Eng. Sci. Technol. Int. J.* **2020**, *23*, 1134–1143. [[CrossRef](#)]
20. Venkatasubramanian, D.; Shanthi, B. An efficient control method for PMSM drive using an optimized indirect matrix converter. *Future Gener. Comput. Syst.* **2019**, *98*, 12–17. [[CrossRef](#)]
21. Zhou, S.; Wang, D.; Li, Y. Parameter identification of permanent magnet synchronous motor based on modified- fuzzy particle swarm optimization. *Energy Rep.* **2023**, *9*, 873–879. [[CrossRef](#)]
22. Zhao, H.; Zuo, W.; Li, Q.; Cheng, Q.; Pan, N.; Zhou, K. Thermal-hydraulic performance optimization of the spiral cooling channel in surface type permanent magnet synchronous motor. *J. Therm. Anal. Calorim.* **2023**, *148*, 10345–10355. [[CrossRef](#)]
23. Sharma, R.; Gupta, V.K.; Khaware, A.; Kamat, V. Efficient CFD Methodology for Optimal Design of Oil Cooled Electric Motor Shaft. *J. Fluid Flow Heat Mass Transf.* **2022**, *9*, 66–75. [[CrossRef](#)]
24. Selema, A.; Ibrahim, M.N.; Sergeant, P. Electrical Machines Winding Technology: Latest Advancements for Transportation Electrification. *Machines* **2022**, *10*, 563. [[CrossRef](#)]
25. ASTM A276/A276M-17; Standar Specification for Stainless Stell Bars and Shapes. ASTM International: West Conshohocken, PA, USA, 2011; p. 7.
26. ASTM E328-20; Standard Test Methods for Stress Relaxation for Materials and Structures. ASTM International: West Conshohocken, PA, USA, 2021; pp. 1–6.
27. A801-14; Standard Specification for Wrought Iron-Cobalt High Magnetic Saturation Alloys. ASTM International: West Conshohocken, PA, USA, 2014; pp. 1–6.
28. Budynas, R.; Keith, N. *Shigley's Mechanical Engineering Design*, 7th ed.; MCGraw Hill: New York, NY, USA, 2008.
29. Peter, C. *Mechanical Design*, 2nd ed.; Elsevier: Amsterdam, The Netherlands, 2004.
30. DIN EN ISO 286-1:2010; Geometrical Product Specifications (GPS)—ISO Code System for Tolerances on Linear Sizes—Part 1: Basis of Tolerances, Deviations and Fits. ISO: Geneva, Switzerland, 2010.

Disclaimer/Publisher's Note: The statements, opinions and data contained in all publications are solely those of the individual author(s) and contributor(s) and not of MDPI and/or the editor(s). MDPI and/or the editor(s) disclaim responsibility for any injury to people or property resulting from any ideas, methods, instructions or products referred to in the content.